

An *ab initio* molecular dynamics study of varied compositions of the LiF-NaF-KF molten salt

Veronica Heyl^a, Benjamin Beeler^{a,b}

^a*North Carolina State University, Raleigh, 27607, NC, USA*

^b*Idaho National Laboratory, Idaho Falls, 83415, ID, USA*

Abstract

With increasing interest in molten salt reactors, there becomes a demand for investigations into thermophysical properties of salt systems. The LiF-NaF-KF (FLiNaK) salt system is a primary candidate for use in these reactors. However, the thermophysical properties of compositions outside the eutectic composition are still largely unknown. In this article, properties of ten unique compositions, including four ternary compositions, are investigated using *ab initio* molecular dynamics simulations across five temperatures between 900 K and 1300 K. The properties of interest are the density, thermal expansion, bulk modulus, compressibility, heat capacity, and enthalpy of mixing. In general, the results were found to be in good agreement with other literature and experimental results. The density and heat capacity had a tendency to be slightly underpredicted. No conclusions could be drawn about the bulk modulus and compressibility in terms of compositional dependence. The thermal expansion had a negative trend with respect to the LiF concentration and no trends were observed for the NaF or KF concentration. The enthalpy of mixing shows minima for the ternary compositions, with the near-equiautomic composition exhibiting the lowest values. This work shows the potential for compositional tailoring in the FLiNaK system to optimize thermophysical properties.

Keywords: molten salts, thermophysical properties, AIMD, FLiNaK

1. Introduction

Molten salts are ionic liquid mixtures at high temperatures with high heat capacity and thermal conductivity. These properties make molten salts useful as a coolant or fuel salt for molten salt reactors (MSRs). Research into MSRs was largely neglected after the experiments by Oak Ridge National Laboratory during the late 1960s[1]. The advantages of an MSR compared to solid fuel reactors are that MSRs do not need traditional fuel fabrication, possess increased intrinsic safety, and have a high working temperature[2]. Because of their benefits, there has been renewed interest in MSRs in the past few years. With this comes the need to characterize molten salts and determine their thermophysical properties, which are required to parameterize complex fluid dynamics and chemical interaction models[1, 3].

The LiF-NaF-KF (FLiNaK) salt system is one of the primary candidates to operate as a coolant salt in MSRs. FLiNaK has been proposed as the heat transfer medium in the Very High-Temperature Reactor, a graphite-moderated, gas-cooled Generation IV concept reactor[4], and is of interest to serve as the primary coolant in MSRE-type designs. FLiNaK

15 is also often utilized as a surrogate for LiF-BeF₂ (FLiBe), which is also of interest in MSRs,
16 but more challenging to explore experimentally due to the toxicity of Be. The volumetric
17 heat capacity for FLiNaK is similar to water but without the issue of critical heat flux due
18 to the large margin to boiling. Additionally, FLiNaK can operate under ambient pressure
19 conditions, allowing for the removal of the high system pressure in water-cooled reactors
20 [5]. Thus, a significant amount of experimental research has been performed on FLiNaK to
21 determine select thermophysical and chemical properties.

22 Frandsen et al. investigated the density as a function of temperature between approx-
23 imately 500[..¹] °C and 1500[..²] °C, the total scattering structure function, and the pair
24 distribution function of the eutectic composition[6]. Anderson et al. collaborated with Oak
25 Ridge National Laboratory to determine the density, equilibrium volume, coefficient of ther-
26 mal expansion, self-diffusion coefficients for constituent ions at 973 K, 1223 K, and 1423
27 K, and the self-diffusion coefficient for solute ions at 973 K[7]. All of these properties were
28 determined at the eutectic composition. Liu et al. studied the microstructures of lutetium
29 fluoride and oxyfluoride structures in eutectic FLiNaK using Raman spectroscopy and den-
30 sity functional theory[8]. Ambrosek et al. used previously acquired experimental data to
31 determine the heat transfer of the eutectic composition in comparison to the Dittus-Boelter
32 correlation[5]. Additional experiments have been performed on the eutectic composition
33 [9, 10, 11].

34 Thermophysical properties are difficult to determine experimentally because of the toxic-
35 ity of salts, the targeted high temperatures, and the cost of the experiment [1]. In lieu of
36 an abundance of high-fidelity experimental data, a computational approach can be pursued
37 to complement and supplement the existing experimental data. Salanne et al. constructed
38 interatomic potentials for mixtures of LiF, NaK, KF, and ZrF₄ and used them for molecular
39 dynamics simulations to evaluate the heat-transfer properties of FLiNaK and NaF-ZrF₄[12].
40 Lee et al. used molecular dynamics to train neutral network forcefields and reparametrized
41 analytical forcefields in order to use large-scale molecular dynamics in the determination
42 of structural and transport properties[13]. Sona et al. used computational fluid dynamics
43 simulations to investigate the flow and heat transfer characteristics of eutectic FLiNaK[14].
44 Recently, *ab initio* molecular dynamics simulations (AIMD) have begun to be explored to
45 determine thermophysical properties, structure, and speciation in FLiNaK[15, 6, 16, 17].

46 The common trend among previous works is the selection of investigating only the eu-
47 tectic composition. As most experimental work has been done on this composition, previous
48 computational work purposely and appropriately chose to focus on the composition that had
49 data available for comparison. While understandable, due to corrosion, changing redox po-
50 tential, and other variables in a reactor environment, the composition of the salt may slightly
51 change as a function of time. Additionally, while the eutectic composition has the minimum
52 melting point for this ternary system, there may be other properties (density, viscosity, heat
53 capacity, etc.) that are more beneficial at non-eutectic compositions, but which are largely
54 unknown[4]. **While both thermophysical and transport properties are required for the correct**
55 **implementation of molten salts in a reactor system, the initial evaluation of thermophysical prop-**

¹removed:

²removed:

56 erties, which are more easily obtainable through both experimental and computational efforts
57 [18, 19, 20], provides an initial step in the full property evaluation of key molten salt systems.
58 Thus, only thermophysical properties are the focus of this manuscript.

59 This work seeks to more fully characterize the thermophysical properties of FLiNaK
60 through a first principles computational investigation of four ternary compositions (including
61 the eutectic), three binary eutectic compositions, and three pure alkali-halide salt con-
62 stituents. The density, bulk modulus, compressibility, heat capacity, thermal expansion, and
63 enthalpy of mixing for each different composition in the FLiNaK system will be determined
64 using appropriate temperatures between 900 K and 1300 K. This is the most extensive in-
65 vestigation of thermophysical properties across the compositional and temperature regimes
66 in the nuclear-relevant molten salt FLiNaK.

67 2. Computational Methods

68 Ten unique compositions (all compositions are stated in mole percent) were studied for
69 the LiF-NaF-KF salt system, including four ternary compositions (eutectic 46-12-42, 16-
70 42-42, 32-34-34, and 42-42-16), three binary eutectic compositions (0-40-60, 51-0-49, and
71 61-39-0), and the three pure alkali-halide salt constituents (LiF, NaF, and KF). The initial
72 structure was prepared by inserting the respective molecules into a supercell via the Packmol
73 package [21], with 100 atoms for the ternary systems and 200 atoms for all other systems.
74 Such system sizes have been shown to produce converged and comparable results for AIMD
75 analyses of molten salts [22, 23]. AIMD simulations were performed using the Vienna *ab*
76 *initio* Simulation Package (VASP)[24, 25, 26]. The temperature range investigated for each
77 composition depended upon the corresponding melting point of that composition, with the
78 ternary system temperatures ranging from 900 K to 1300 K, binary system temperatures
79 from 1000 K to 1300 K, and the pure constituent temperatures from 1100 K to 1300 K. The
80 energy cutoff was 600 eV, which is 100 eV higher than the recommended maximum for the
81 pseudopotentials utilized, and the electronic optimization criterion was 10^{-3} eV. Convergence
82 testing was performed with more fine energy convergence criteria to ensure that the results
83 were not affected by the choice of electronic optimization. A $1 \times 1 \times 1$ k-point mesh was used,
84 as this has been shown to be sufficient in prior simulations for molten salts with similarly
85 sized supercells[18, 15]. The vdW-DF2 van der Waals functional was used to account for the
86 dispersion interactions[27, 28]. While there are many choices of dispersion interactions avail-
87 able within VASP, this specific choice was made due to its ability to replicate the properties
88 of various chloride salts[18]. A brief examination of the DFT-D3 dispersion correction term
89 [29] was also explored, which did not show superior predictions.

90 In the Open Visualization Tool (OVITO)[30], the initial structures were verified to have
91 no bonds shorter than 1.5 Å, indicating a reasonable initial guess. The structures were
92 equilibrated using VASP at each temperature studied. The initial equilibrium simulation for
93 each composition occurred at 1100 K. The energy was evaluated versus time to check if the
94 system was equilibrated. If the slope of the running average was approximately zero, the
95 structure was considered to be at equilibrium. If not, the simulation was continued until it
96 was determined that equilibrium was reached. Typically, equilibration takes approximately
97 10-15 ps.

98 Utilizing the equilibrated structures, the system was further evolved at different specified

99 volumes to obtain the pressure as a function of volume. The systems were equilibrated for a
 100 further 4 ps, with time-averaging to determine the energy and pressure over the final 3 ps.
 101 At least six data points were included for each composition and temperature, ensuring that
 102 the pressures ranged from -2 to +10 kbar, with at least one pressure greater than 5 kbar.
 103 This is in accordance with a prior procedure utilized[18]. Five simulations were performed
 104 for each unique volume for statistical significance. Thus, for a given composition and tem-
 105 perature, approximately thirty simulations were performed. The pressure as a function of
 106 the volume, shown in fig. 1a, was determined by fitting a quadratic equation, allowing for
 107 the determination of the volume at which the pressure is zero.

108 The zero pressure volume, along with the mass, was used to calculate the density. The
 109 parabolic fit of the volume-pressure curve was used to calculate the bulk modulus and com-
 110 pressibility:

$$K = -V \left(\frac{\partial P}{\partial V} \right)_{P=0} = \frac{1}{\beta} \quad (1)$$

111 where K is the bulk modulus, V is the volume, P is the pressure, and β is the compressibility.

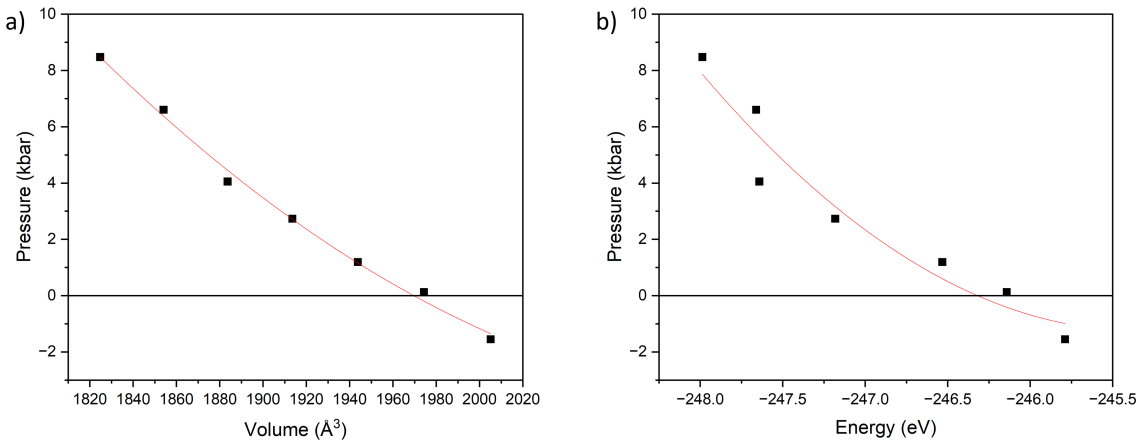


Figure 1: An example of the a) pressure as a function of volume and b) pressure as a function of energy for the 16-42-42 mol% composition at 1000 K.

112 In a similar manner used to determine the density, the heat capacity can also be found.
 113 The pressure as a function of potential energy, shown in fig. 1b, was determined by fitting
 114 a quadratic equation, allowing for the determination of the potential energy at which the
 115 pressure is zero. This zero-pressure potential energy is then added to the kinetic energy,
 116 and the total energy is plotted versus temperature. A linear function is fit to the data to
 117 obtain the total energy as a function of temperature. From this, the heat capacity can be
 118 determined:

$$C_p = \lim_{\Delta T \rightarrow 0} \frac{\partial E}{\partial T} \quad (2)$$

119 where C_p is the heat capacity, T is the absolute temperature, and E is the total energy. It
 120 was verified that a linear function adequately represented the data, indicating a constant
 121 heat capacity over the temperature range investigated.

¹²² The thermal expansion is determined by analyzing the zero-pressure volume as a function
¹²³ of temperature, treating the coefficient of thermal expansion (α) as:

$$\alpha = \frac{1}{V_0} \left(\frac{\partial V}{\partial T} \right)_p \quad (3)$$

¹²⁴ where V_0 is a reference volume at the lowest temperature explored for each composition.

¹²⁵ The enthalpy of mixing is determined from the potential energy of the mixed system and
¹²⁶ the three binary salts:

$$\Delta H^{mix} = \frac{E_{ABC}}{M_{ABC}} - \frac{x_A E_A}{M_A} - \frac{x_B E_B}{M_B} - \frac{x_C E_C}{M_C} \quad (4)$$

¹²⁷ where M_i is the number of molecules in the system, E_A , E_B , and E_C are the potential energies
¹²⁸ of the reference systems (LiF, NaF, and KF), E_{ABC} is the potential energy of the ternary
¹²⁹ system, and x_A , x_B , and x_C are the mole fraction of the respective reference salts in the
¹³⁰ mixture. This same equation can be applied to binary salt mixtures, reducing from four
¹³¹ terms to three. While assumptions can be made to incorporate entropic effects to determine
¹³² the free energy of mixing, such a step was not taken due to inherent assumptions required
¹³³ for ideal solution-type behavior.

¹³⁴ The binary and unary salt systems were equilibrated in a strictly NPT ensemble, easing
¹³⁵ some of the computational burden of exploring varied salt complexes, but limiting the ability
¹³⁶ to explore volume-dependent phenomena, such as the compressibility. There are no statis-
¹³⁷ tically significant differences in calculated thermodynamic quantities from the utilization of
¹³⁸ an NPT versus an NVT ensemble.

¹³⁹ 3. Results

¹⁴⁰ 3.1. Density and Thermal Expansion

¹⁴¹ The density of each composition studied is displayed as a function of temperature in fig. 2.
¹⁴² It should be noted that for all densities reported here, there is an approximate error of 0.05
¹⁴³ g/cc. For all compositions, the density decreases with increasing temperature. This is in line
¹⁴⁴ with the inversely proportional relationship between density and temperature. The minimum
¹⁴⁵ density is observed for the pure LiF system, while the maximum density is observed for the
¹⁴⁶ NaF system. All of the densities fall within a range of approximately 0.25 g/cc, with the
¹⁴⁷ intermediate compositions having a much narrower range of only about 0.1 g/cc. Thus, the
¹⁴⁸ maximum variation for the ternary compositions is approximately 5%. All data presented is
¹⁴⁹ also included in tabular form in the appendix.

¹⁵⁰ The density can be analyzed by composition, as in fig. 3, where there is an overall decrease in
¹⁵¹ the density as the percent of LiF increases. The opposite occurs in fig. 3b, where the density
¹⁵² increases as the percent of NaF increases. Looking at fig. 3c, there appears to be little effect as
¹⁵³ the percent of KF changes. This seems to be reasonable, as the density of LiF is the lowest, the
¹⁵⁴ density of NaF is the highest, and the density of KF is at an intermediate value between the
¹⁵⁵ other two. It should be emphasized that in fig. 3, ternary, binary, and unary salt densities are
¹⁵⁶ all included. For the three temperatures at which all ten compositions were studied, ternary
¹⁵⁷ heatmaps, shown in fig. 4, were generated to better visualize the effects of the changing

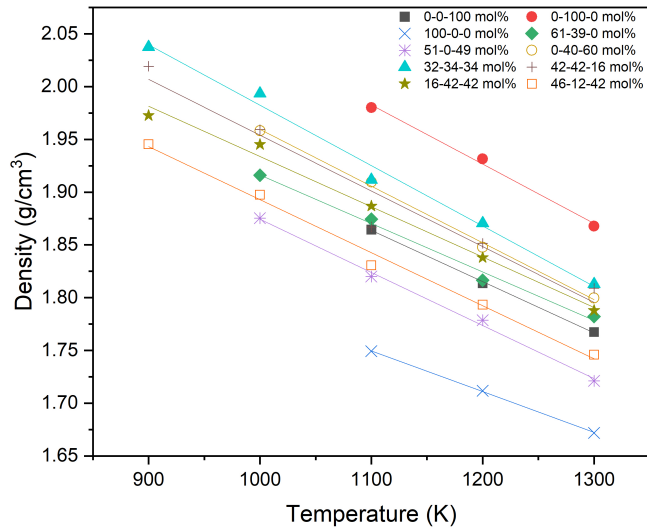


Figure 2: The density (g/cm^3) versus temperature (K) of all compositions studied (LiF-NaF-KF mol%).

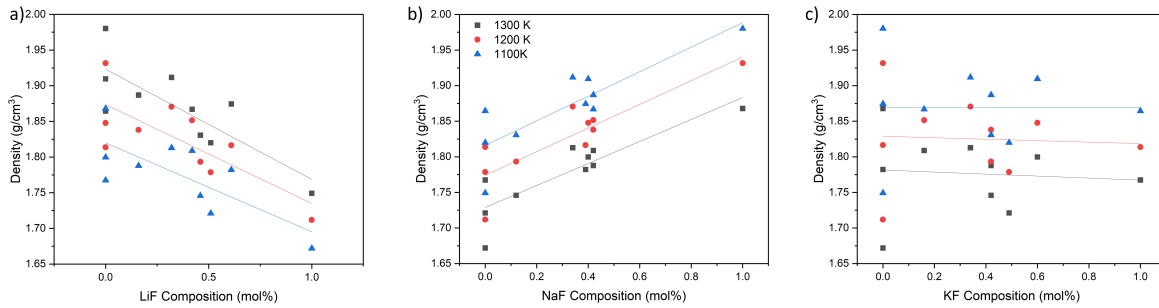


Figure 3: The density (g/cm^3) as a function of the composition of a) LiF (mol%), b) NaF (mol%), and c) KF (mol%) for different FLiNaK salts.

composition. While a limited number of compositions were utilized for the construction of the ternary density heat maps, they can clearly illustrate the dependence upon the composition. The composition of the mixture with respect to the LiF-NaF binary system is the primary determining factor for the density of the ternary, with the KF composition having nearly a negligible effect. It appears that density decreases more sharply as the composition nears LiF than the density decreases as the NaF composition increases, but additional data points at intermediate compositions would be required to verify these behaviors. For the four ternary phases, the eutectic is somewhat the outlier, possessing the least NaF and thus exhibiting the lowest density. The lower density of the eutectic composition compared to other ternary compositions may or may not be preferable. Regardless, these variations are somewhat minor. These conclusions hold across the temperature range studied. More complex density surfaces may be present but are not identifiable with the limited number of compositions studied here.

Experimental densities are available for comparison with the eutectic composition. When

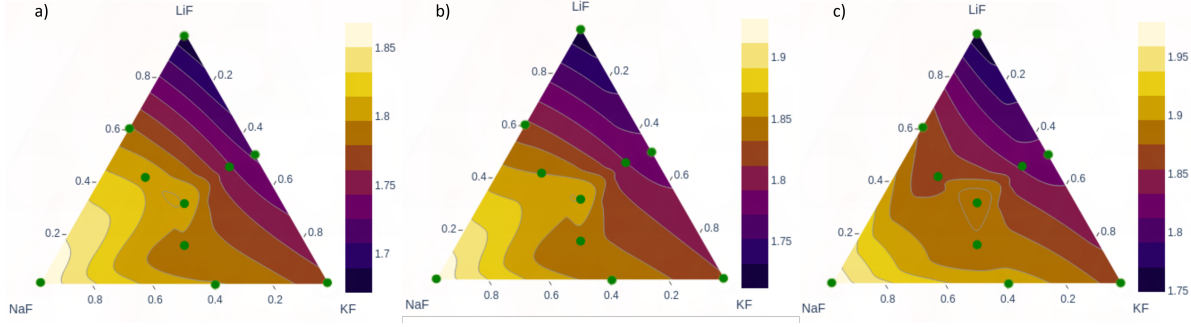


Figure 4: Ternary heatmap of the density (g/cm^3) of FLiNaK at a) 1300 K, b) 1200 K, and c) 1100 K.

171 compared to experimental values from Janz [31] (shown in fig. 5a), this work slightly under-
 172 predicts the density at all temperatures. The data deviates on average by 0.05 g/cc from
 173 Janz. For the individual salt endpoints (LiF, NaF, KF), the comparisons with experiments
 174 are shown in fig. 5b. There is a consistent, but minor, underprediction for the densities at all
 175 temperatures, but the change in the density with temperature shows good agreement, as the
 176 average deviation across all individual salts is 0.06 g/cc. As experimental measurements often
 177 report uncertainties on the order of 1-5% [32], there is general confidence in the magnitude
 178 and trends of the density with varying compositions. **The error bars shown in fig. 5 include a**
 179 **2% error from experiments, and a propagated computational error accounting for the scatter in**
 180 **each individual data point and the error from the quadratic fit, as illustrated in fig. 1. The error**
 181 **bars all predicted densities overlap with the error bars from experiments for all compositions and**
 182 **temperatures.**

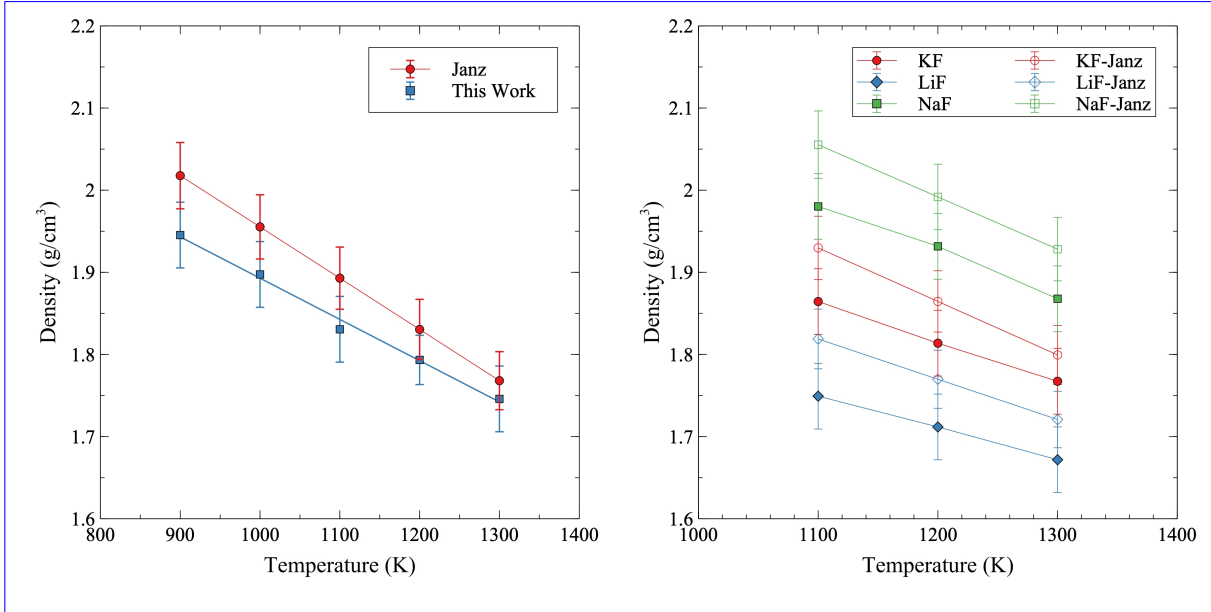


Figure 5: Comparison of density, g/cm^3 , versus temperature, K, of a) the eutectic composition with literature[31] and b) pure salts with literature[32].

183 The thermal expansion can be taken from the slope of the density in fig. 2 with respect
 184 to temperature (eq. (3)). The thermal expansion coefficient is plotted versus composition in

185 fig. 6. The trends of the thermal expansion with respect to composition are not as strong as
 186 those for density. The LiF concentration in fig. 6a has a negative impact on the coefficient
 187 of thermal expansion. However, as shown in fig. 6b and fig. 6c, there is not a statistically
 188 significant impact on the thermal expansion of varying compositions of NaF or KF. However,
 189 with increasing NaF and KF, there is a minor increase in the thermal expansion. The
 190 minimum thermal expansion of the four ternary compositions occurs at 16-42-42 mol %, and
 191 the maximum occurs at 32-34-34 mol %. When considering only the ternary compositions,
 192 the previously stated trends do not apply as there is no statistically significant relationship
 193 between the composition of the unary salts and thermal expansion.

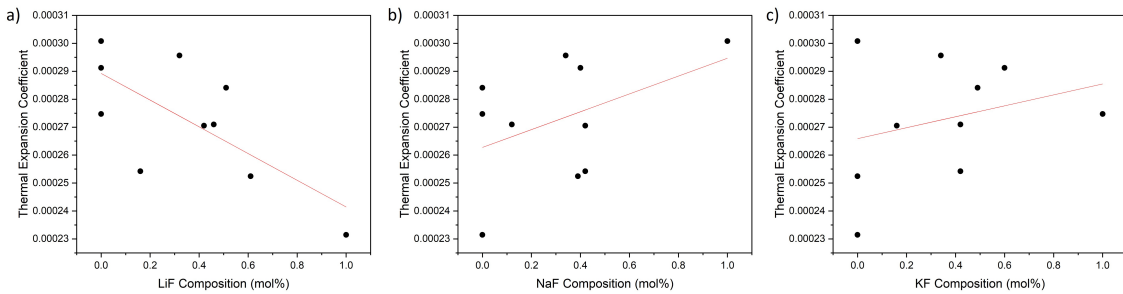


Figure 6: The thermal expansion coefficient versus the composition of a) LiF (mol%), b) KF (mol%), and c) NaF (mol%) for different FLiNaK salts.

194 3.2. Bulk Modulus and Compressibility

195 The bulk modulus and the compressibility are shown in fig. 7. It should be emphasized
 196 that the compressibility is the inverse of the bulk modulus. Both are shown here for com-
 197 pleteness. The degree of compressibility of a fluid has strong implications for its dynamics.
 198 As expected, the compressibility increases as the temperature increases. There is significant
 199 scatter in the data, which makes drawing specific conclusions regarding compositional de-
 200 pendence difficult, but generally, the eutectic composition has an intermediate value of the
 201 compressibility. The near equiatomic ternary salt has the lowest compressibility, and the
 202 low LiF content salt has the highest compressibility. Compared to two binary chloride salts
 203 (LiCl-KCl [18] and NaCl-MgCl₂ [33]), the ternary compositions of FLiNaK display a lower
 204 value of the compressibility. Only ternary salts are included here as non-ternary composi-
 205 tions were analyzed in an NPT ensemble, which did not allow for the evaluation of the bulk
 206 modulus.

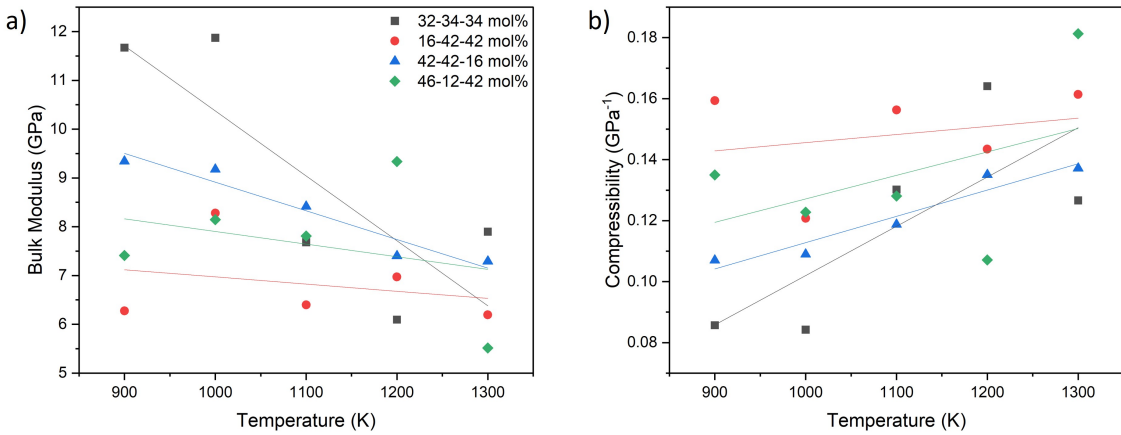


Figure 7: a) Bulk modulus and b) compressibility of the four ternary compositions versus temperature

207 3.3. Heat Capacity and Enthalpy of Mixing

208 Heat capacity is a required parameter for thermal hydraulics models describing heat trans-
 209 port in molten salt systems[3]. The heat capacity for FLiNaK is best visualized as a ternary
 210 heatmap, shown in fig. 8. The heat capacity is greatest around the middle compositions
 211 and decreases as the system moves towards the three pure alkali-halide salt constituents. As
 212 stated, the exact contour locations may vary from their depiction here due to the limited
 213 number of ternary compositions, but the variance in the heat capacity with composition, in
 214 that a near equiatomic mixture has the highest heat capacity, is quite consistent. The total
 215 energy from AIMD simulations shows a linear dependence, thus the heat capacity is effectively
 216 constant over the investigated temperature range. Williams et al. report the heat capacity
 217 of the eutectic composition to be 77.9 J/mol-K at 973 K[34], which compares quite favorably
 218 to the calculated value of 67.6 J/mol-K from this work. Compared to the reported literature
 219 value, this work underpredicts the heat capacity by 13.2%, but is neglecting the electronic
 220 contribution to the heat capacity, which, if included, would decrease the discrepancy. **This**
 221 **is because the total heat capacity is a combination of the electron and phonon contributions to**
 222 **the heat capacity [35], and including the electronic component will serve to increase the predicted**
 223 **value of the heat capacity.** It should be noted that heat capacity measurements are notoriously
 224 difficult in molten salts, and often are in disagreement with one another [36]. Generally, a
 225 higher heat capacity is preferable for thermal hydraulics applications, and thus this work
 226 points to a potential benefit of utilizing near-equiatomic compositions of FLiNaK.

227 The enthalpy of mixing is plotted against each of the pure alkali-halide salt constituents
 228 in fig. 9. Considering that this figure includes both ternary and binary compounds, the char-
 229 acteristic inverse hull shape is not present. However, intermediate compositions display the
 230 lowest enthalpy of mixing, with the near-equiatomic (32-34-34) composition exhibiting the
 231 global lowest energy. Including entropic effects to yield a free energy of formation was beyond
 232 the scope of this work, but it is anticipated that the near equiatomic composition would likely
 233 display the largest entropy, and thus the lowest free energy. Unfortunately, there is no exper-
 234 imental data for comparison. Additionally, prior computational investigations were typically

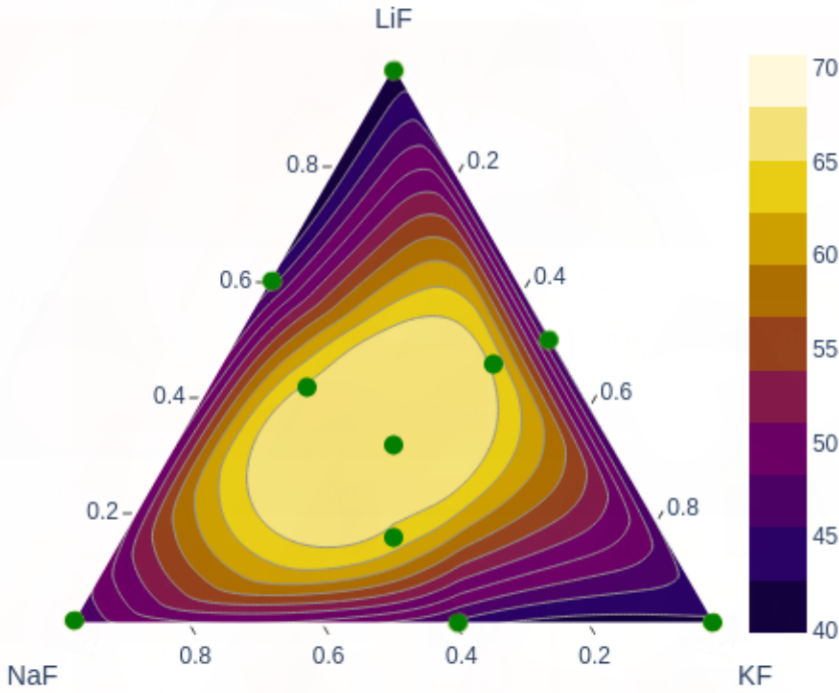


Figure 8: Ternary heatmap of the heat capacity of FLiNaK (J/mol-K).

235 restricted to the eutectic composition and did not explore the unary salt components, which
 236 prevented them from determining the enthalpy of formation. Experimental and additional
 237 computational studies are warranted to validate these results.

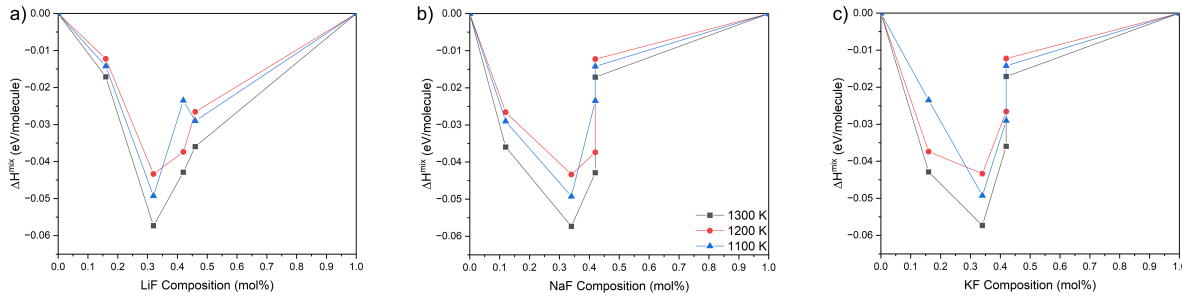


Figure 9: Graph of the enthalpy of mixing, eV/molecule, versus composition of a) LiF (mol%), b) NaF (mol%), and c) KF (mol%).

238 3.4. Coordination Analysis

239 The local atomic structure is analyzed by means of the radial pair distribution function
 240 (RDF). The RDF, or $g(r)$, measures the probability of finding a particle at distance r given
 241 that there is a particle at position $r = 0$. The peak of the RDF for each pair is the most
 242 probable location of the first-nearest-neighbor (1nn). The RDF for eutectic LiF-NaF-KF is
 243 shown in fig. 10 at 900 K. Note that not all pair-wise interactions are shown in fig. 10, to aid

244 in readability. Also, this RDF constitutes a time average over 3 ps of a given simulation at
 245 the zero-pressure volume at 900 K. The 1nn distance is then determined and compared to
 246 an x-ray diffraction study conducted at 793 K in table 1. Generally, the RDF compares very
 247 favorably to the experimental results, as well as a prior computational study [6]. The most
 248 significant difference being for the F-F peak, which is overestimated by approximately 0.09 Å.
 249 However, the experimental results assumed a Gaussian distribution for their analysis, which
 250 may induce small errors, and reported a mean square-root displacement of 0.41 Å, indicating
 251 a broad peak, which is in accordance with these results and provides additional confidence
 252 in the accuracy of the simulations. The RDFs of the other ternary systems were analyzed to
 253 identify potential variations with somewhat minor compositional differences. The individual
 254 pair distances did not statistically change for the primary species, however, the F-F bond did
 255 show some variance depending upon the system, with the low Li concentration (16-42-42)
 256 displaying the longest F-F 1nn distance (3.33 Å) and the eutectic displaying the shortest F-F
 257 bond 1nn distance (3.14 Å) (table A.3). There is not a clear correlation between F-F 1nn
 258 distance and density, which one might expect. However, there is a negative linear correlation
 259 ($R^2=0.98$) with the Li content, with greater Li content exhibiting shorter F-F 1nn distances.
 260 These minor structural variations would need to be confirmed via experiments and may
 261 provide insight into dynamical properties related to the distribution of F atoms in FLiNaK
 262 salts.

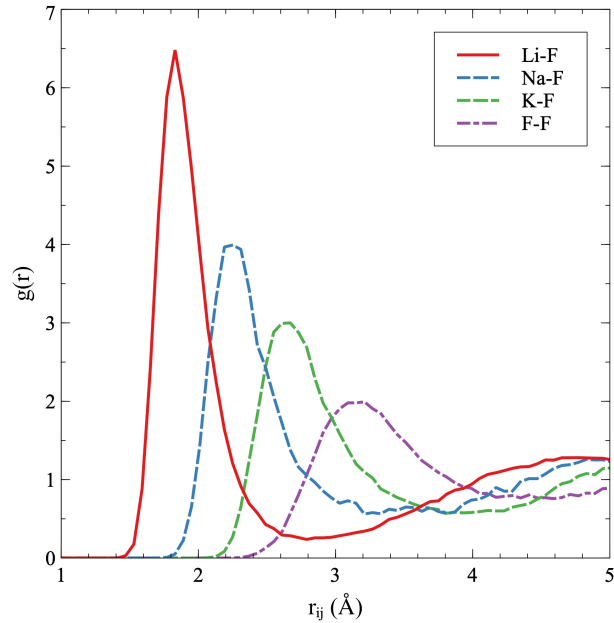


Figure 10: Partial radial distribution functions for eutectic LiF-NaF-KF at 900 K.

Table 1: First nearest neighbor distances for eutectic LiF-NaF-KF at 900 K. Results are compared against experiment at 793 K [37].

Pair	r_{ij} (Å)	r_{ij} (Å)[37]
Li-F	1.82	1.83
Na-F	2.23	2.18
K-F	2.64	2.59
F-F	3.14	3.05

263 4. Conclusion

264 To characterize the thermophysical properties of FLiNaK, a first principles computa-
 265 tional investigation was performed for four ternary compositions, three binary eutectic com-
 266 positions, and three pure alkali-halide salt constituents. The computational results of the
 267 density slightly underpredicted the experimental values at all temperatures for the eutectic
 268 and pure salt compositions. However, generally good agreement is observed. The density
 269 is positively correlated with the NaF concentration and negatively correlated with the LiF
 270 concentration. The thermal expansion was determined to decrease with increasing LiF con-
 271 centration, but there was no statistically significant dependence on NaF or KF. The large
 272 scatter in the data for the bulk modulus and compressibility resulted in an inability to draw
 273 specific conclusions about compositional dependence, however, the compressibility increased
 274 with the temperature, as expected, and displays a magnitude lower than comparable chloride
 275 salts. The results for the heat capacity, like the density, underpredicted the literature value,
 276 but are likely within experimental uncertainties. In the enthalpy of mixing versus composi-
 277 tion, the ternary compositions display the lowest formation energy, with the near equiatomic
 278 composition possessing the minimum.

279 As the interest in molten salt reactors is renewed, there is a need for thermophysical
 280 properties of salt systems at varied compositions rather than just the eutectic composition.
 281 Currently, these properties are largely unknown, but can be elucidated through first principles
 282 methods. This work has shown that some thermophysical properties can exhibit significant
 283 differences with relatively minor compositional variance, indicating the potential for tailoring
 284 even well-known molten salt systems to target specific property behaviors. Further exper-
 285 imental work is necessary to validate the results presented in this manuscript, providing
 286 further confidence in the ability of first principles methods to explore the vast composition
 287 and temperature space relevant to molten salts in nuclear applications.

288 5. Acknowledgements

289 This work was supported through the NC State Nuclear Engineering Undergraduate Re-
 290 search Scholar Program with funding courtesy of the College of Engineering Enhancement
 291 Fee. This work is also supported through the INL Laboratory Directed Research and Develop-
 292 ment (LDRD) Program under DOE Idaho Operations Office Contract DE-AC07-05ID14517.
 293 This research made use of the resources of the High-Performance Computing Center at Idaho
 294 National Laboratory, which is supported by the Office of Nuclear Energy of the U.S. Depart-
 295 ment of Energy and the Nuclear Science User Facilities.

²⁹⁶ Appendix A.

Table A.1: The density (g/cm^3) of LiF-NaF-KF at different temperatures.

Composition (LiF-NaF-KF)	900 K	1000 K	1100 K	1200 K	1300 K
eutectic 46-12-42	1.95	1.90	1.83	1.79	1.75
16-42-42	1.97	1.95	1.89	1.84	1.79
32-34-34	2.04	1.99	1.91	1.87	1.81
42-42-16	2.02	1.96	1.87	1.85	1.81
0-40-60	-	1.96	1.91	1.85	1.80
51-0-49	-	1.88	1.82	1.78	1.72
61-39-0	-	1.92	1.87	1.82	1.78
100-0-0	-	-	1.75	1.71	1.67
0-100-0	-	-	1.98	1.93	1.87
0-0-100	-	-	1.86	1.81	1.77

Table A.2: The coefficient of thermal expansion (α), compressibility (β at 1100 K), heat capacity (C_P), and enthalpy of mixing (ΔH_{mix} at 1300 K) of LiF-NaF-KF.

Composition (LiF-NaF-KF)	$\alpha \times 10^{-4}$	$\beta (\text{GPa}^{-1})$	$C_P (\text{J/mol-K})$	$\Delta H_{mix}(\text{eV/molecule})$
eutectic 46-12-42	2.88	0.128	67.6	-0.027
16-42-42	2.66	0.121	66.8	-0.017
32-34-34	3.15	0.130	70.7	-0.057
42-42-16	2.93	0.119	68.3	-0.043
0-40-60	2.91	-	43.1	-0.007
51-0-49	2.84	-	43.0	-0.043
61-39-0	2.52	-	42.0	-0.028
100-0-0	2.31	-	39.9	-
0-100-0	3.01	-	44.4	-
0-0-100	2.75	-	41.9	-

Table A.3: The first-nearest-neighbor distances of the ternary LiF-NaF-KF salts at 900K.

Composition (LiF-NaF-KF)	F-F 1nn distance (Å)
eutectic 46-12-42	3.14
16-42-42	3.33
32-34-34	3.21
42-42-16	3.15

297 References

- [1] T. Porter, M. Vaka, P. Steenblik, D. Della Corte, Computational methods to simulate molten salt thermophysical properties, *Commun Chem* 5 (2022) 69. doi:10.1038/s42004-022-00684-6.
 URL <https://www.nature.com/articles/s42004-022-00684-6>
- [2] G. Locatelli, M. Mancini, N. Todeschini, Generation iv nuclear reactors: Current status and future prospects, *Energy Policy* 61 (2013) 1503–1520. doi:10.1016/j.enpol.2013.06.101.
 URL <https://www.sciencedirect.com/science/article/pii/S0301421513006083>
- [3] Freile, Ramiro, Kimber, Mark, Influence of molten salt-(flinak) thermophysical properties on a heated tube using cfd rans turbulence modeling of an experimental testbed, *EPJ Nuclear Sci. Technol.* 5 (2019) 16. doi:10.1051/epjn/2019027.
 URL <https://doi.org/10.1051/epjn/2019027>
- [4] O. Beneš, R. Konings, Thermodynamic properties and phase diagrams of fluoride salts for nuclear applications, *Journal of Fluorine Chemistry* (2009) 22–29doi:<https://doi.org/10.1016/j.jfluchem.2008.07.014>.
 URL <https://www.sciencedirect.com/science/article/pii/S0022113908002030>
- [5] J. Ambrosek, M. Anderson, K. Sridharan, T. Allen, Current status of knowledge of the fluoride salt (flinak) heat transfer, *Nuclear Technology* 165 (2009) 166–173. doi:10.13182/NT165-166.
 URL <https://www.tandfonline.com/doi/full/10.13182/NT165-166>
- [6] B. A. Frandsen, S. D. Nickerson, A. D. Clark, A. Solano, R. Baral, J. Williams, J. Neufeind, M. Memmott, The structure of molten flinak, *Journal of Nuclear Materials* 537 (2020) 152219. doi:10.1016/j.jnucmat.2020.152219.
 URL <https://www.sciencedirect.com/science/article/pii/S0022311520304736>
- [7] M. Anderson, K. Sridharan, D. Morgan, P. Peterson, P. Calderoni, R. Scheele, A. Casekka, B. McNamara, Heat transfer salts for nuclear reactor systems - chemistry control, corrosion mitigation, and modeling, Tech. Rep. Project No. 10-905, University of Wisconsin, Madison (1 2015). doi:10.2172/1169921.
 URL <https://www.osti.gov/biblio/1169921>

- 327 [8] X. Liu, Y. Li, B. Wang, C. Wang, Raman and density functional theory stud-
328 ies of lutecium fluoride and oxyfluoride structures in molten flinak, Spectrochim-
329 ica Acta Part A: Molecular and Biomolecular Spectroscopy 251 (2021) 119435.
330 doi:10.1016/j.saa.2021.119435.
331 URL <https://www.sciencedirect.com/science/article/pii/S1386142521000111>
- 332 [9] H. W. Hoffman, J. Lones, Fused salt heat transfer. part ii. forced convection heat trans-
333 fer in circular tubes containing naf-kf-lif eutectic, Tech. Rep. ORNL-1777, Oak Ridge
334 National Laboratory (2 1955). doi:10.2172/4016896.
335 URL <https://www.osti.gov/biblio/4016896>
- 336 [10] D. Holcomb, S. Cetiner, An overview of liquid-fluoride-salt heat transport sys-
337 tems, Tech. Rep. ORNL/TM-2010/156, Oak Ridge National Laboratory (10 2010).
338 doi:10.2172/990239.
- 339 [11] G. L. Yoder, Jr, D. W. Heatherly, D. F. Williams, Y. M. Elkassabgi, J. Caja, M. Caja,
340 J. Jordan, R. Salinas, Liquid fluoride salt experimentation using a small natural circu-
341 lation cell, Tech. Rep. ORNL/TM-2014/56, Oak Ridge National Laboratory (4 2014).
342 doi:10.2172/1130418.
343 URL <https://www.osti.gov/biblio/1130418>
- 344 [12] M. Salanne, C. Simon, P. Turq, P. A. Madden, Heat-transport properties of molten
345 fluorides: Determination from first-principles, Journal of Fluorine Chemistry 130 (2009)
346 38–44. doi:10.1016/j.jfluchem.2008.07.013.
- 347 [13] S.-C. Lee, Y. Zhai, Z. Li, N. P. Walter, M. Rose, B. J. Heuser, Y. Z, Comparative
348 studies of the structural and transport properties of molten salt flinak using the machine-
349 learned neural network and reparametrized classical forcefields, The Journal of Physical
350 Chemistry B 125 (2021) 10562–10570. doi:10.1021/acs.jpcb.1c05608.
351 URL <https://pubs.acs.org/doi/10.1021/acs.jpcb.1c05608>
- 352 [14] C. Sona, M. A. Khanwale, C. S. Mathpati, A. Borgohain, N. K. Maheshwari, In-
353 vestigation of flow and heat characteristics and structure identification of flinak
354 in pipe using cfd simulations, Applied Thermal Engineering 70 (2014) 451–461.
355 doi:10.1016/j.applthermaleng.2014.05.043.
- 356 [15] H. Nam, A. Bengtson, K. Vörtler, S. Saha, R. Sakidja, D. Morgan, First-principles
357 molecular dynamics modeling of the molten fluoride salt with cr solute, Journal of Nu-
358 clear Materials 449 (2014) 148–157. doi:10.1016/j.jnucmat.2014.03.014.
359 URL <https://www.sciencedirect.com/science/article/pii/S0022311514001238>
- 360 [16] A. D. Clark, W. L. Lee, A. R. Solano, T. B. Williams, G. S. Meyer, G. J. Tait,
361 B. C. Battraw, S. D. Nickerson, Complexation of mo in flinak molten salt: Insight
362 from ab initio molecular dynamics, Journal of Physical Chemistry B 125 (2020).
363 doi:10.1021/acs.jpcb.0c07354.
- 364 [17] D. Sprouster, G. Zheng, S.-C. Lee, D. Olds, C. Agca, J. McFarlane, Y. Z, B. Khaykovich,
365 Molecular structure and phase equilibria of molten fluoride salt with and without

- 366 dissolved cesium: Flinak–csf (5 mol %), ACS Applied Energy Materials 5 (2022).
367 doi:10.1021/acsaem.2c00544.
- 368 [18] K. Duemmler, Y. Lin, M. Woods, T. Karlsson, R. Gakhar, B. Beeler,
369 Evaluation of thermophysical properties of the licl-kcl system via ab initio
370 and experimental methods, Journal of Nuclear Materials 559 (2022) 153414.
371 doi:<https://doi.org/10.1016/j.jnucmat.2021.153414>.
372 URL <https://www.sciencedirect.com/science/article/pii/S0022311521006346>
- 373 [19] K. Duemmler, M. Woods, T. Karlsson, R. Gakhar, B. Beeler, First-principles-derived
374 transport properties of molten chloride salts, Journal of Nuclear Materials 585 (2023)
375 154601. doi:<https://doi.org/10.1016/j.jnucmat.2023.154601>.
376 URL <https://www.sciencedirect.com/science/article/pii/S0022311523003689>
- 377 [20] D. Zhao, L. Yan, T. Jiang, S. Peng, B. Yue, On the viscosity of molten salts and molten
378 salt mixtures and its temperature dependence, Journal of Energy Storage 61 (2023)
379 106707. doi:<https://doi.org/10.1016/j.est.2023.106707>.
380 URL <https://www.sciencedirect.com/science/article/pii/S2352152X23001044>
- 381 [21] L. Martínez, R. Andrade, E. G. Birgin, J. M. Martínez, Packmol: A
382 package for building initial configurations for molecular dynamics sim-
383 ulations, Journal of Computational Chemistry 30 (13) (2009) 2157–
384 2164. arXiv:<https://onlinelibrary.wiley.com/doi/pdf/10.1002/jcc.21224>,
385 doi:<https://doi.org/10.1002/jcc.21224>.
386 URL <https://onlinelibrary.wiley.com/doi/abs/10.1002/jcc.21224>
- 387 [22] A. Bengtson, H. O. Nam, S. Saha, R. Sakidja, D. Morgan, First-principles molecular
388 dynamics modeling of the licl–kcl molten salt system, Computational Materials Science
389 83 (2014). doi:10.1016/j.commatsci.2013.10.043.
390 URL <https://www.sciencedirect.com/science/article/pii/S0927025613006630>
- 391 [23] D. Andersson, B. Beeler, Ab initio molecular dynamics (aimd) simulations of
392 nacl, ucl3 and nacl-ucl3 molten salts, Journal of Nuclear Materials 568 (2022).
393 doi:10.1016/j.jnucmat.2022.153836.
394 URL <https://www.sciencedirect.com/science/article/pii/S0022311522003221>
- 395 [24] G. Kresse, J. Hafner, Ab initio molecular dynamics for liquid metals, Phys. Rev. B 47
396 (1993) 558–561. doi:10.1103/PhysRevB.47.558.
397 URL <https://link.aps.org/doi/10.1103/PhysRevB.47.558>
- 398 [25] G. Kresse, J. Furthmüller, Efficiency of ab-initio total energy calculations for metals and
399 semiconductors using a plane-wave basis set, Computational Materials Science 6 (1996)
400 15–50. doi:[https://doi.org/10.1016/0927-0256\(96\)00008-0](https://doi.org/10.1016/0927-0256(96)00008-0).
401 URL <https://www.sciencedirect.com/science/article/pii/0927025696000080>
- 402 [26] G. Kresse, J. Furthmüller, Efficient iterative schemes for ab initio total-energy
403 calculations using a plane-wave basis set, Phys. Rev. B 54 (1996) 11169–11186.

- 404 doi:10.1103/PhysRevB.54.11169.
405 URL <https://link.aps.org/doi/10.1103/PhysRevB.54.11169>
- 406 [27] J. Klimeš, D. R. Bowler, A. Michaelides, Chemical accuracy for the van der waals
407 density functional, *Journal of Physics: Condensed Matter* 22 (2) (2009) 022201.
408 doi:10.1088/0953-8984/22/2/022201.
- 409 [28] J. Klimeš, D. R. Bowler, A. Michaelides, Van der waals density functionals applied to
410 solids, *Physical Review B* 83 (19) (may 2011). doi:10.1103/physrevb.83.195131.
411 URL <https://doi.org/10.1103%2Fphysrevb.83.195131>
- 412 [29] S. Grimme, J. Antony, S. Ehrlich, H. Krieg, A consistent and accurate ab
413 initio parametrization of density functional dispersion correction (dft-d) for the
414 94 elements h-pu, *The Journal of Chemical Physics* 132 (15) (2010) 154104.
415 arXiv:<https://doi.org/10.1063/1.3382344>, doi:10.1063/1.3382344.
416 URL <https://doi.org/10.1063/1.3382344>
- 417 [30] A. Stukowski, Visualization and analysis of atomistic simulation data with OVITO-the
418 Open Visualization Tool, *MODELLING AND SIMULATION IN MATERIALS SCI-
419 ENCE AND ENGINEERING* 18 (1) (JAN 2010). doi:10.1088/0965-0393/18/1/015012.
- 420 [31] G. Janz, R. Tomkins, Physical properties data compilations relevant to energy storage.
421 iv. molten salts: Data on additional single and multi-component salt systems, *Tech.
422 Rep. NSRDS-NBS* 61, National Bureau of Standards (1981).
- 423 [32] G. Janz, Thermodynamic and transport properties for molten salts: Correlation equa-
424 tions for critically evaluated density, surface tension, electrical conductance, and viscos-
425 ity data, *Journal of Physical and Chemical Reference Data* 17 (1988).
- 426 [33] K. Duemmler, M. Woods, T. Karlsson, R. Gakhar, B. Beeler, An ab
427 initio molecular dynamics investigation of the thermophysical properties
428 of molten nacl-mgcl₂, *Journal of Nuclear Materials* 570 (2022) 153916.
429 doi:<https://doi.org/10.1016/j.jnucmat.2022.153916>.
430 URL <https://www.sciencedirect.com/science/article/pii/S0022311522004020>
- 431 [34] D. F. Williams, Assessment of candidate molten salt coolants for the advanced high
432 temperature reactor (ahtr), *Tech. Rep. ORNL/TM-2006/12*, Oak Ridge National Lab-
433 oratory (3 2006). doi:10.2172/885975.
434 URL <https://www.osti.gov/biblio/885975>
- 435 [35] A. Moore, B. Beeler, C. Deo, M. Baskes, M. Okuniewski, Atomistic modeling of high
436 temperature uranium–zirconium alloy structure and thermodynamics, *Journal of Nu-
437 clear Materials* 467 (2015) 802–819. doi:<https://doi.org/10.1016/j.jnucmat.2015.10.016>.
438 URL <https://www.sciencedirect.com/science/article/pii/S0022311515302683>
- 439 [36] S. G. Robertson, R. Wiser, W. Yang, D. Kang, S. Choi, E. Baglietto, M. P. Short, The
440 curious temperature dependence of fluoride molten salt thermal conductivity, *Journal of*

- 441 Applied Physics 131 (22), 225102 (06 2022). arXiv:https://pubs.aip.org/aip/jap/article-pdf/doi/10.1063/5.0088059/16508374/225102_1_online.pdf, doi:10.1063/5.0088059.
442
443 URL <https://doi.org/10.1063/5.0088059>
- 444 [37] K. Igarashi, Y. Okamoto, J. Mochinaga, H. Ohno, X-ray diffraction study of molten
445 eutectic lif–naf–kf mixture, J. Chem. Soc., Faraday Trans. 1 84 (1988) 4407–4415.
446 doi:10.1039/F19888404407.
447 URL <http://dx.doi.org/10.1039/F19888404407>